Korean J. Chem. Eng., **30**(1), 111-122 (2013)
DOI: 10.1007/s11814-012-0096-y

Characterization of modified sawdust, kinetic and equilibrium study about methylene blue adsorption in batch mode

Weihua Zou†, Hongjuan Bai, Shuaipeng Gao, and Ke Li

School of Chemical Engineering and Energy, Zhengzhou University, 100# of Kexue Road, Zhengzhou 450001, P. R. China
(*Received 18 November 2011 • accepted 18 June 2012*)

Abstract−Methylene blue (MB) biosorption by citric acid modified pine sawdust (Pinus tabulaeformis) was studied from aqueous solutions. Batch experiments were conducted to determine the biosorption properties of the biomass. The Langmuir isotherm equation could fit the equilibrium data. The maximal equilibrium quantity of MB from Langmuir model was 111.46 mg g^{-1} at 293 K. The Elovich model adequately described the kinetic data in comparison to the pseudo-first-order model and pseudo-second-order model; the process involving rate-controlling step is very complex involving both boundary layer and intra-particle diffusion processes. The effective diffusion parameter D_i and D_f values were estimated at different initial concentration, and the average values were determined to be 5.76×10^{-8} and 2.12×10^{-7} cm^2 s^{-1}. Thermodynamic parameters showed that the adsorption of methylene blue onto pine sawdust biomass was feasible, spontaneous and endothermic under studied conditions. The physical and chemical properties of the biosorbent were determined by SEM, TG-DSC, XRD, and the point of zero charge (pH_{pzc}) and the nature of biomass-dye interactions were evaluated by FTIR analysis, which showed the participation of COOH, OH and NH_2 groups in the biosorption process. Biosorbents could be regenerated using 0.01 mol L^{-1} HCl solution at least three cycles, with up to 90% recovery. Thus, the biomass used in this work proved to be effective for the treatment of MB bearing aqueous solutions.

Key words: Adsorption, Modified Sawdust (CAMS), Methylene Blue (MB), Adsorption Kinetics, Equilibrium, Mechanisms

INTRODUCTION

Water pollution due to synthetic dyes is a major concern. Many industries such as leather tanning, paint and pigments, paper and pulp and textile generate a considerable amount of colored effiuent. More than 10,000 chemically different dyes are being manufactured. The world dyestuff and dye intermediates are estimated at a production around 7×10^8 kg per annum [1]. Due to the dyes' synthetic origin and complex molecular structure, which can make them more stable and difficult to be biodegraded once they enter the water, it is no longer good and sometimes difficult to treat [2]. Dye effluents can cause several problems: (i) dyes can have acute or chronic effects on exposed organisms, which depends on exposure time and dye concentration; and (ii) the dyes' absorption and reflection of sunlight entering the water can interfere with the growth of bacteria to levels sufficient to biologically degrade impurities in the water and start the food chain [3]. Most of these dyes are synthetic and usually composed of aromatic rings in their structures. They make the dyes carcinogenic and mutagenic, inert and non-biodegradable when discharged into waste streams [4]. Hence, it is necessary to remove dyes from dyeing wastewater before it is discharged into water bodies.

The main techniques of dye removal from the effluent include sedimentation, filtration technology, chemical treatment, oxidation, electrochemical methodology, etc., but due to high cost and high energy inputs, inapplicability to small-scale sector of developing countries, and producing undesirable by-products, few of the techniques are accepted [2]. Hence, it is essential to search for a low-cost, effective, and environment-friendly technology to remove dyes from aqueous solutions. Adsorption is one such means. Commercial activated carbon is an effective adsorbent, but its high cost inhibits its large-scale application. So it is necessary to find alternative low-cost to substitute activated carbon [1]. Large numbers of studies have shown that agricultural by-products such as orange peel [5], pine tree leaves [1], rejected tea [6], mansonia wood sawdust [4], wheat straw [7], peanut hull [8], banana peel [9], rice husk [10], can be used as low-cost adsorbents to remove the dye of wastewater. Generally, the sorption capacities of crude agricultural by-products are low. To improve the adsorption capacity of these by-products, chemical modification has been used [11]. Wood powder does not noticeably swell in water and does not decompose upon prolonged contact with water. It can be used as a low-cost adsorbent largely due to its lignocellulosic composition. It contains abundant lignin, cellulose, hemicellulose and some functional groups such as carboxyl, hydroxyl, phenolic and amide groups in its structure, which make the adsorption processes possible [12]. A number of publications have reported on the use of wood sawdust to remove contamination from solution [12,13]. But the use of modified sawdust with citric acid (CAMS) as adsorbent for removal of MB from solution is not studied.

The objective of this work was to modify sawdust with citric acid to enhance the adsorption capacity of the by-product for selected methylene blue (MB) from aqueous solution. The characterization of natural sawdust (NS) and modified sawdust was analyzed by scanning electron microscopy (SEM), thermo-gravimetric analysis

†To whom correspondence should be addressed.
E-mail: whzou@zzu.edu.cn

and differential scanning calorimetry (TGA-DSC), X-ray diffraction (XRD), and Fourier transform infrared spectroscopy (FTIR) method. The equilibrium, kinetic data and thermodynamic parameters were also investigated to understand the adsorption mechanism of MB onto CAMS, especially the regeneration of the dye-loaded sawdust.

MATERIALS AND METHODS

1. Adsorbate - Methylene Blue

Methylene blue (MB) ($C_{16}H_{18}ClN_3S{\cdot}3H_2O$, FW: 373.90) (chemical grade reagent) was used as an adsorbate without further purification. Stock solution was prepared by dissolving 0.5 g of MB in 1,000 mL distilled water. The experimental solutions were obtained by diluting the dye stock solution in accurate proportions to the need concentration. MB is a kind of phenothiazine dye, with the chemical structure as follows:

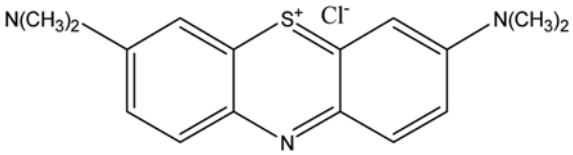

2. Adsorbent Preparation and Characterization

Natural sawdust (NS) was obtained from a local wood processing factory in Zhengzhou City, P. R. China. The sawdust was washed with distilled water for several times to remove the dirt particles, and then dried at 50 °C for 24 h in an oven. The dry sawdust was sieved to obtain particle size in the range of 20-40 mesh for chemical modification.

The citric acid modified sawdust (CAMS) was prepared according to the modified method [14]. Raw sawdust was mixed with a 0.5 mol L^{-1} solution of citric acid at the ratio of 1 : 12 (sawdust/acid, w/v) and stirred continuously for 30 min at room temperature. The acid/sawdust slurry was placed in a stainless steel tray and dried at 50 °C in a forced air oven for 24 h. Then the oven temperature was raised to 120 °C for 90 min to make the thermo-chemical esterication proceed between acid and sawdust. After cooling, the CAMS was washed with distilled water until the liquid did not turn turbid when 0.1 mol L^{-1} lead (II) nitrate was dropped in. After filtration, the modified sawdust was suspended in 0.1 mol L^{-1} NaOH solution at suitable ratio and stirred for 60 min. Then the sample was washed thoroughly with distilled water until the sample was neutralized and dried in the oven at 50 °C for 24 h. Finally, the resulting adsorbent was stored in air-tight container for further use to adsorption experiments.

The photomicrography of the exterior surface of NS and CAMS was obtained by SEM (JEOL JSM-7500F, Japan). The thermal behavior of sawdust was obtained by using a thermogravimetric analyzer (STA 409 PC, German). About 10 mg of NS was heated to 800 °C in oxidant atmosphere at 10 min^{-1} temperature rate. The mineralogy of the sample was characterized by X-ray diffraction (XRD) (Tokyo Shibaura Model ADG-01E). The FT-IR of adsorbent was performed as follows: 5 mg of NS and CAMS was mixed with 100 mg of spectroscopy grade KBr, dried at irradiation by FTIR lamp, and pressed into a small tablet. FT-IR spectra were recorded on a PE-1710 FTIR (USA) instrument in the absorption mode with a resolution of 4 cm^{-1}, in the range of 4,000-400 cm^{-1}.

The pH_{pzc} of an adsorbent determines the pH at which the adsorbent surface has net electrical neutrality. The determination of the pH_{pzc} of the CAMS was as follows [15]: 10 mL of 0.01 mol L^{-1} NaCl solution was placed in a closed conical ask. The pH was adjusted to a value between 2 and 11 by adding HCl or NaOH solutions. Then, 0.05 g of CAMS was added and the final pH measured after 10 h under agitation at room temperature. The pH_{pzc} is the point where the curve $pH_{initial}$ vs. pH_{final} crosses the line $pH_{initial}$=pH_{final}.

3. Adsorption Experiments

Isothermal adsorption experiments were performed by batch technique in a single system at 293, 303 and 313 K, respectively. A series of 50 mL conical flasks were used and each flask contained CAMS at a mass loading of 2 g L^{-1} in the presence of 10 mL of the MB solution at an initial concentration within the range 25-500 mg L^{-1}, and then the flasks were sealed to prevent a change of volume of the solution during the experiments. The conical flasks were agitated on an orbital shaker at 100 rpm for 480 min. After adsorption, the MB solution was separated from the adsorbent. Kinetic studies were performed by loading 2 g L^{-1} CAMS into several sets of conical flasks containing 10 mL of MB solution of known initial concentration. Flasks were taken from the shakers at predetermined time intervals and the remaining concentration of MB in solution estimated. The effect of pH on the amount of dye removal was analyzed over the pH range 2-11. The pH value was adjusted by the addition of 1 mol L^{-1} NaOH or HCl solutions as necessary. The effects of salt concentration on MB uptake were examined by NaCl, KCl and $CaCl_2$ solutions (0.01-0.1 mol L^{-1}) to adjust the ionic strength.

The concentration of MB in solution was determined with a Shimadzu UV-3000 UV spectrophotometer to monitor the absorbance changes at the maximum absorbance wavelength (665 nm). The percentage dye removal (% P) and the amount of dye adsorbed per unit weight of adsorbent at time t (q_t, mg g^{-1}) and at equilibrium (q_e, mg g^{-1}) were calculated using the equations as follows, respectively:

$$\%P = \frac{C_0 - C_e}{C_0} \times 100 \quad (1)$$

$$q_t = \frac{(C_0 - C_t)v}{m} \quad (2)$$

$$q_e = \frac{(C_0 - C_e)v}{m} \quad (3)$$

where v (L) is the volume of MB solution, C_0 (mg L^{-1}) is the initial concentration of MB, C_t (mg L^{-1}) is the concentration of MB at a given time t, C_e (mg L^{-1}) is the initial concentration of MB at equilibrium and m (g) is the dry weight of the adsorbents.

The relative parameters for isotherm and kinetic equation were obtained using the χ^2 relationship between the calculated and experimental data employing non-linear regression analysis. The calculated expression for χ^2 may be written as:

$$\chi^2 = \sum \frac{(q_{e,exp.} - q_{e,calc.})^2}{q_{e,calc.}} \quad (4)$$

where $q_{e,calc.}$ is the predicted (calculated) quantity of MB adsorbed onto CAMS according to the various adsorption models and $q_{e,exp.}$ relates to the experimental data.

4. Desorption Tests

To determine the reusability of CAMS, consecutive adsorption-desorption cycles were repeated three times. For this, 0.1 mol L^{-1} HCl, 0.01 mol L^{-1} HCl and 10% absolute ethanol solution, was used as the desorbing agent, respectively. The CAMS loaded with MB was placed in the desorbing medium and was constantly stirred on a rotary shaker at 100 rpm for 480 min at 283 K. After each cycle of adsorption and desorption, the adsorbent was washed with distilled water and reconditioned for adsorption in the succeeding cycle.

RESULTS AND DISCUSSION

1. Characterization of NS and CAMS

1-1. SEM of NS ad CAMS

Scanning electron micrographs of NS and CAMS are shown in Fig. 1. The NS's surface texture was smooth with vertical grooves on the surface of NS. The smooth fractured surface of NS is due to the high amount of lignin in the compound middle lamellae between the cell walls, while vertical grooves are due to removing all cell wall components, causing a widespread thinning of the wall [16]. The surface of CAMS is rougher than that of NS. The morphology of this material can facilitate the adsorption of dyes due to the irregularity, thus making possible the adsorption of adsorbate in different parts of this material.

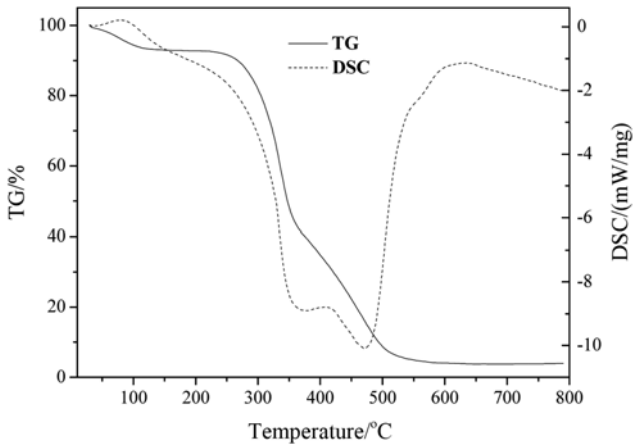

Fig. 2. Curves of thermo-gravimetric analysis (TGA) and differential scanning calorimetry (DSC) of natural sawdust.

1-2. TGA-DSC Analysis of Natural Sawdust

Like all green plant biomass, NS is composed of cellulose and lignin. Fig. 2 shows the curve of TG and DSC of NS.

The overall mass loss during thermo-gravimetric analyses can be divided into steps related to moisture, cellulose and lignin which are shown in Fig. 2. Thus, from Fig. 2, by heating sawdust to 190 °C,

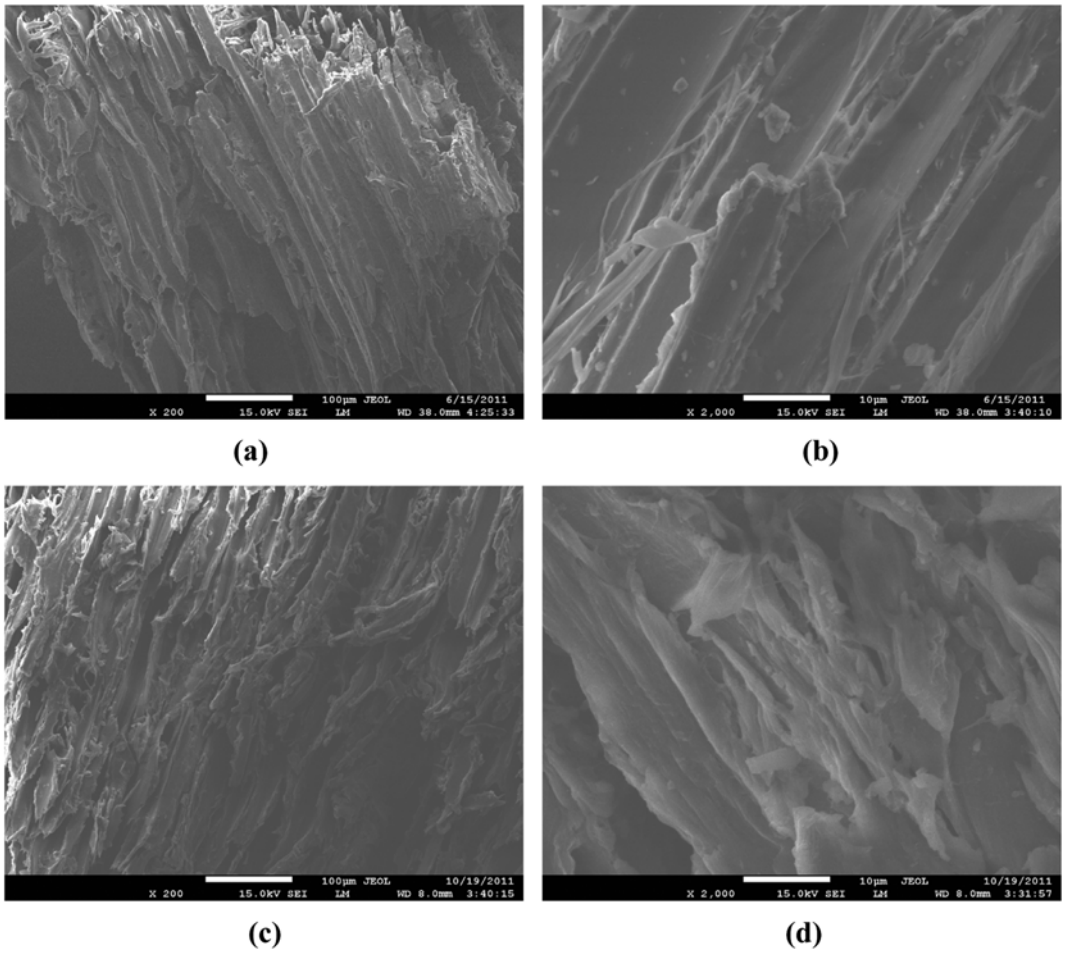

Fig. 1. SEM of NS (a), (b) and CAMS (c), (d).

the mass loss was 7.19%, which was due to the elimination of moisture retained in this material. From 190 to 270 °C, mass loss was insignicant. Then the second step of pyrolysis was obtained when the temperature was varied from 270 to 375 °C. In this step, a higher mass loss of 52.69% was observed. The behavior of the pyrolysis curve at this temperature indicates cellulose decomposition, as well as loss of the remaining adsorbed water. Lignin decomposition occurs in the 375 to 520 °C range whose mass loss was 36.17%, thus indicating that this structure presents higher stability than cellulose. Finally, there was no mass loss when the temperature was increased to 800 °C. This result indicated the presence of oxides (mainly those of aluminum and silicon), which are stable at higher temperatures [17].

From the DSC curve in Fig. 2, the max peaks at 375 °C and 470 °C were observed by exothermic decomposed reaction from cellulose and lignin, respectively.

1-3. FTIR Analysis

Fourier-transform infrared (FT-IR) spectroscopy is used for identifying surface functional groups which are capable of adsorbing dye ions [17]. The FT-IR spectrum of NS, CAMS and CAMS with MB adsorbed is shown in Fig. 3.

From Fig. 3, the spectra display a number of absorption peaks, indicating the complex nature of the material. The broad absorption peaks at ca. 3,417 cm^{-1} indicate the existence of bonded hydroxy groups on the surface of the sawdust. This band is associated with the vibrations of the linked hydroxy groups in cellulose and lignin, and adsorbed water on the sawdust surface. The peaks observed at 2,926 and 1,374 cm^{-1} are assigned to the stretch and bending vibration of the C-H bond in the methyl groups, respectively. Similarly, the peaks located at 1,733 and 1,654 cm^{-1} are characteristic of carbonyl group stretching in aldehydes and ketones [18]. The peak at ca. 1,422 cm^{-1} is also attributed to the stretch vibration of C-O associated with the carboxyl group. The strong C-O band at 1,031 cm^{-1} is specific to the lignin component from wood sawdust. Fig. 3 also indicates that modification of the sawdust led to an increase the absorption band corresponding to the stretch vibration of the carboxyl group at ca. 1,735 cm^{-1}, with the positions of some peaks being changed after modification. These results show that CAMS possesses more carboxyl groups than raw sawdust and has higher physical stability and surface activity.

Band intensity is a function of the change in the electrical dipole moment and also the total number of related bonds in the sample. Thus, the C-O group band was more intense than that of the C=O group, possibly as a result of more C-O groups being present in the adsorbent [19]. These groups may function as proton donors and, as a consequence, deprotonated hydroxy and carboxyl groups may be involved in coordination with positive dye ions. Dissolved MB ions are positively charged and will undergo attraction on approaching the anionic CAMS structure. On this basis, it is expected that CAMS will show a strong adsorption affinity towards MB ions [10].

The FTIR spectra also revealed that there were various functional groups detected on the surface of CAMS sample before and after adsorption. There are some peaks that were shifted, and disappeared. As seen in Fig. 3, three signicant bands increase of the functional groups on the CAMS was detected at the bands of 1,598, 1,331 and 883 cm^{-1} which indicated the bonded C=O groups, aromatic nitro compound and C-C group. These three signicant bands in the spectrum indicate the possible involvement of that functional group on the surface of CAMS in MB adsorption process.

1-4. XRD of NS and CAMS

The XRD spectra of NS and CAMS are shown in Fig. 4. The XRD pattern of raw sawdust shows a typical spectrum of cellulosic material, which has main and secondary peaks at 2θ of ca. 22° and 16°, respectively [20]. The main peak is an indicator of the presence of highly organized crystalline cellulose, while the secondary peak is a measure of a less organized polysaccharide structure. After

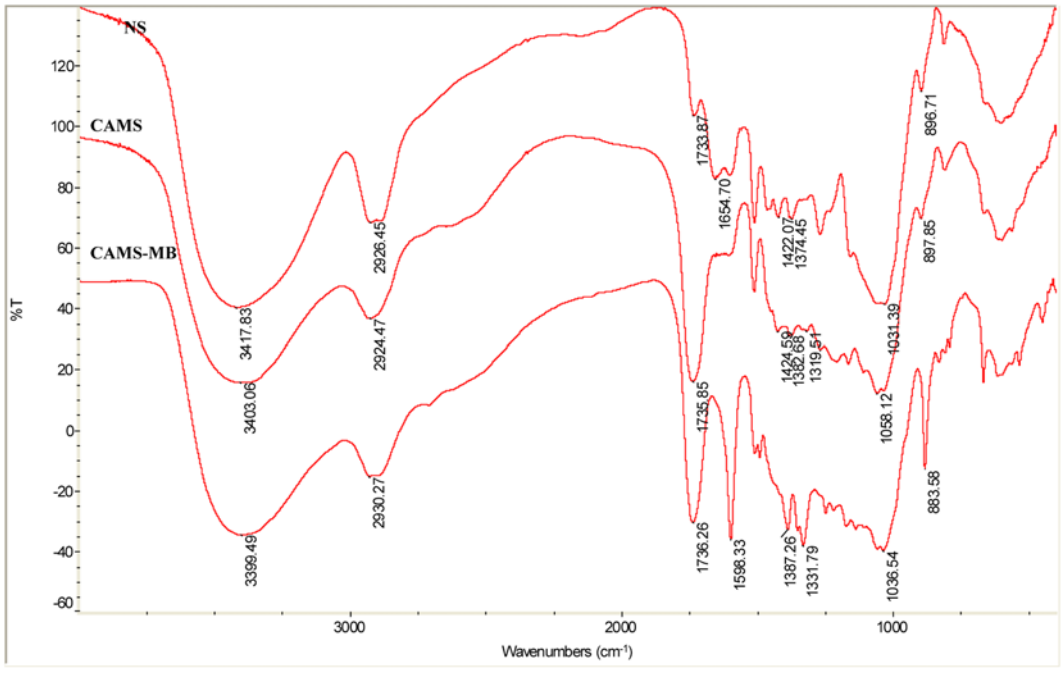

Fig. 3. Fourier-transform infrared spectra of NS, CAMS and CAMS adsorbed MB.

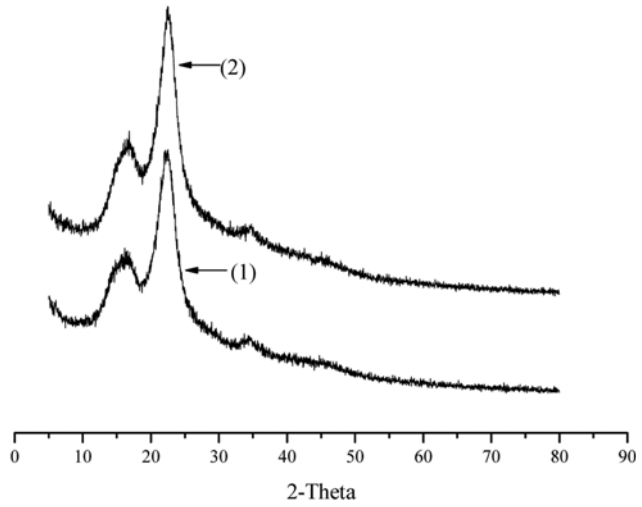

Fig. 4. The XRD of NS (1) and CAMS (2).

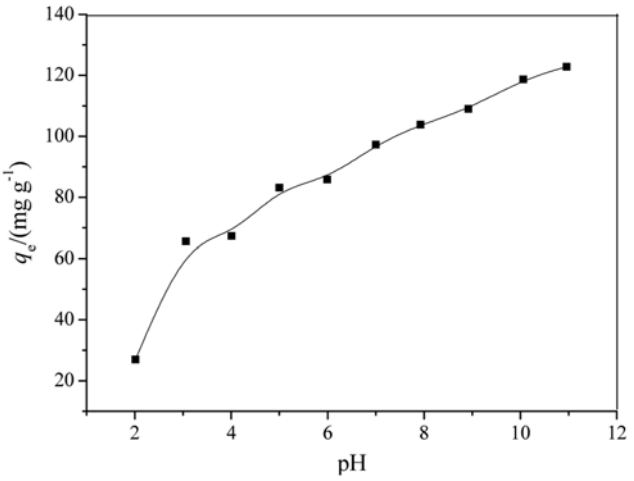

Fig. 6. Effect of initial pH of the solution on the adsorption MB onto CAMS (C_o=250 mg L^{-1}; CAMS: 2 g L^{-1}; 480 min; 293 K).

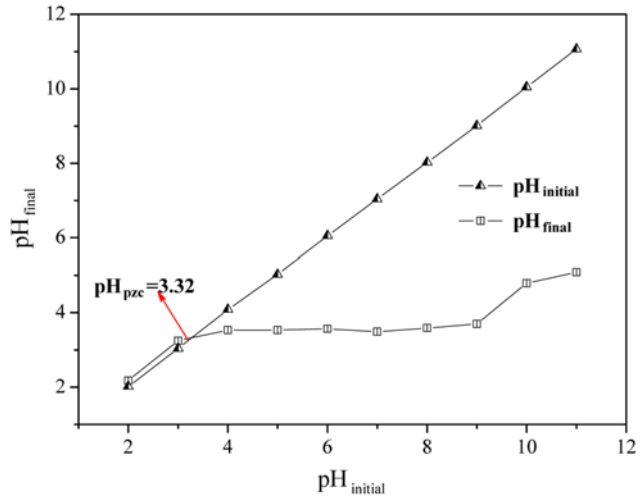

Fig. 5. The variation of point of zero charge with equilibrium pH of CAMS suspensions.

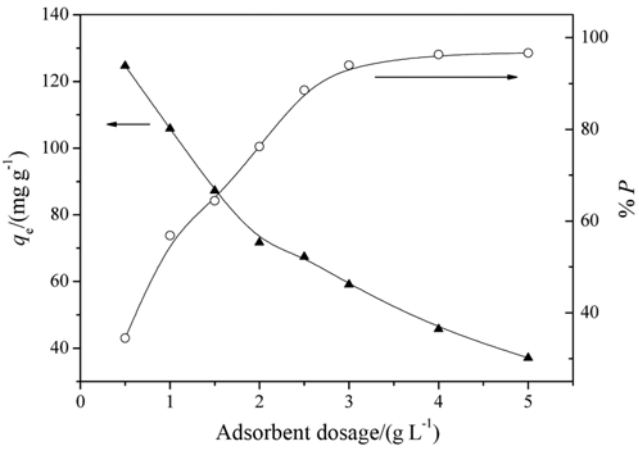

Fig. 7. Effect of adsorbent dose on the adsorption of MB onto CAMS (C_o=250 mg L^{-1}; CAMS: 2 g L^{-1}; 480 min; 293 K).

carboxyl group esterication, the height of the main and secondary peak in XRD diagram increased, indicating that the crystallinity of esteried adsorbent actually increased.

1-5. The Point of Zero Charge (pH_{pzc})

Fig. 5 illustrates the point of zero charge (pzc) of CAMS. The pH_{pzc} of CAMS was found to be 3.32. The surface of CAMS was positively charged below pH 3.32, while it acquired a negative charge above this pH value.

2. Influence of Operation Conditions on Batch Adsorption of MB

2-1. Effect of Initial pH

The effect of initial pH of MB solution was analyzed over the range from 2 to 11. The result is shown in Fig. 6. As seen there, when pH increased from 2 to 11 for MB, the amount of dye adsorbed increased from 26.95 to 122.87 mg g^{-1}. Several reasons may be attributed to MB adsorption behavior of the adsorbent relative to solution pH.

The increase may be related to the formation of negative surface charges on the adsorbent which is influenced by the solution pH. Both negative and positively charged surface sites exist in aqueous solution, depending on the solution pH. When solution pH<pH_{pzc}, the surface of CAMS is positively charged and attractive to anions. The practical functional group of CAMS is carboxyl group. The presence of excess H^+ ions could restrain the ionization of the carboxyl group, so the non-ionic form of carboxyl group, -COOH, was presented. The adsorption capacity of dye ions was small because of the absence of electrostatic interaction. When solution pH>pH_{pzc}, the surface of CAMS is negatively charged and can attract cations from the solution The carboxyl group is turned into -COO^-, a significantly high electrostatic attraction exists between the negatively charged surface of CAMS and cationic dye molecules, leading to maximum dye adsorption. Similar results were reported for the adsorption of cationic dye from aqueous solution on biosorbent [21, 22]. In this paper, the initial pH of the aqueous was set to 6.5.

2-2. Effect of Adsorbent Dose

The effect of the adsorbent dose on the amount of MB adsorbed by CAMS and its corresponding percentage removal from solution are shown in Fig. 7.

From Fig. 7, it was observed that the percentage removal increased from 34.4% to 96.6% with an increase in adsorbent dose from 0.5 to 5 g L^{-1}. Increasing the dosage of CAMS led to an increase in the number of sorbent surface area and sorption sites available for sorbent-solute interaction. However, with the further increase in the amount of the adsorbent from 4 g L^{-1} to 5 g L^{-1}, the percentage removal of MB only varied between 96.3% and 96.6%. Because at higher adsorbent dose, the adsorption sites of adsorbent increased and the adsorption percent also increased. When the concentration of MB in solution was lower, the adsorption-desorption process achieved the dynamic equilibrium, resulting in the percentage removal of MB did not go beyond 96.6% when the dose increased from 4 to 5 g L^{-1}. Also, the adsorption capacity decreased from 124 to 37 mg g^{-1} as the adsorbent dose increased from 0.5 to 5 g L^{-1}. This could be ascribed to the difference in the concentration gradient between the solute concentration in solution and on the surface of the adsorbent. Another possible reason was the overlapping or aggregation of the adsorbent surface area available for MB adsorption and a corresponding increase in the diffusion path length [10].

2-3. Effect of Common Salt Concentration and Competitive Ions

Different amounts of various salts are contained in the dye-laden wastewaters. These salts can result in a high ionic strength which may affect the performance of the adsorption process. The effect of salt concentration of MB onto CAMS was studied by the addition of chloride to the dye solution. The result is shown in Fig. 8.

As seen in Fig. 8, with the increasing of the salt concentrations, the adsorptive capacity of dye removal decreased. From Fig. 8, when the concentration of NaCl, KCl and $CaCl_2$ increased from 0 to 0.1 mol L^{-1}, the value of q_e decreased from 85.84 to 75.85, 64.97 and 36.64 mg g^{-1}, respectively. This result indicated that the adsorbing efficiency decreased with the concentrations of NaCl, KCl and $CaCl_2$ increasing in the MB solution, respectively. This may be ascribed to the competitive effect between MB ions and cations from the salt for the sites available for the adsorption process. As Ca^{2+} had more contribution to ionic strength and more positive charge than Na^+ and K^+, the effect of Ca^{2+} on adsorption was more serious than Na^+ and K^+ at the same mole concentration, and compared to K^+, Na^+ had little effect on the adsorption of MB.

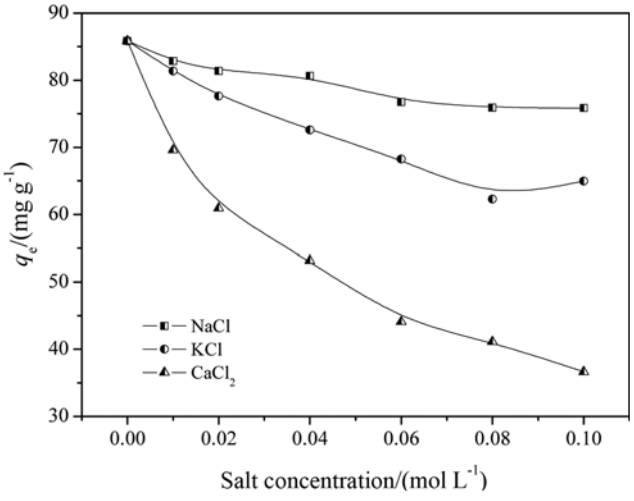

Fig. 8. Effect of salt concentration on the adsorption of MB onto CAMS (C_o=250 mg L^{-1}; CAMS: 2 g L^{-1}; 480 min; 293 K).

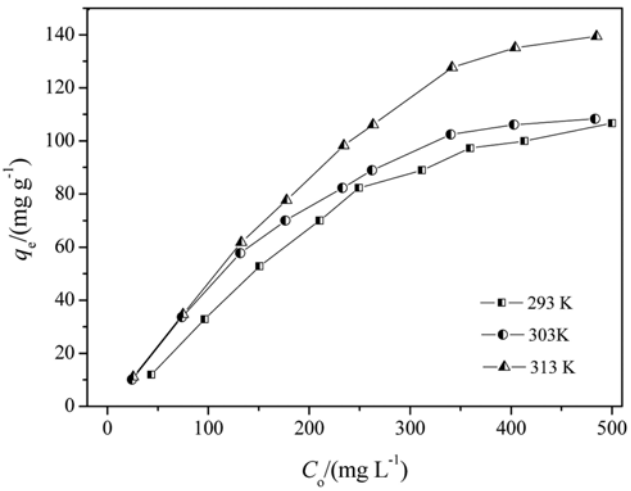

Fig. 9. Effect of initial dye concentration and temperature on adsorption of MB onto CAMS.

2-4. Effect of Initial Dye Concentration and Temperature

The effect of temperature and initial dye concentration is shown in Fig. 9. With increasing of the initial MB concentration ranging from 25 to 500 mg L^{-1}, the value of q_e increased from 11.97 to 106.68 mg g^{-1} at 293 K. The reason was that the initial adsorbate concentration provided an important driving force to overcome all mass transfer resistances of MB between the aqueous and solid phases [1]. Due to the interaction between dyes and adsorbents increasing with the values of C_o, the adsorption uptake of MB can also increase.

Temperature is also an important parameter in the adsorption process. The bigger adsorptive capacity of dyes was also observed in the higher temperature range. This result was expected because higher temperature would result in higher diffusion rates accompanied by decreasing viscosity and density of the solute, which can enhance the extent of adsorption. The results also indicated that this system was an endothermic process and the adsorption of MB onto CAMS was favored at high temperature. The positive effect of temperature on the observed adsorption can be related to the enhancement of the diffusion rate of MB through the boundary layer due to decrease of solution viscosity as well as mobility of dye molecules with the increase of temperature, and within internal pores of the CAMS particles [23,24]. In other words, considering a fixed concentration of MB and CAMS, a greater number of dye molecules were transferred from the bulk solution onto adsorbent particles, resulting in both an increase of removal percentage and adsorption capacity [25]. Similar results were previously reported for temperature on the removal of MB onto different adsorbents [26,27].

2-5. Adsorption Isotherms

Analysis of the equilibrium data is significant to develop an equation which precisely represents the results and can be used for optimizing the design of an adsorption system. In the present study, the Langmuir, Freundlich, Redlich-Peterson, and Dubinin-Radushkevich models were applied to describe the adsorption equilibrium. All relative parameters of the isotherm equations, the values of R^2 and χ^2 are listed in Table 1, respectively. Fig. 10 also shows the experimental equilibrium data and the fitted equilibrium curves obtained from the application of various isotherm models at different temperature.

Table 1. Isotherm constants for MB sorption onto CAMS at different temperatures using non-linear regressive method

T/K	293	303	313
Langmuir			
q_m (mg g^{-1})	111.46	114.40	156.6
K_L	0.075	0.053	0.051
R_L	0.031-0.235	0.038-0.438	0.039-0.435
R^2	0.962	0.977	0.974
χ^2	40.24	29.18	64.23
Freundlich			
K_F	31.0	22.0	26.4
1/n	0.233	0.300	0.336
R^2	0.784	0.925	0.912
χ^2	229.6	94.78	214.8
Redlich-Peterson			
A	6.979	7.667	8.965
B	0.065	0.103	0.072
g	0.989	0.919	0.956
R^2	0.944	0.982	0.975
χ^2	22.09	26.11	71.01
Dubinin-Radushkevich			
q_m (mg g^{-1})	115.84	119.02	160.28
E (kJ mol^{-1})	16.02	15.22	15.12
R^2	0.7300	0.8840	0.8649
χ^2	286.4	146.8	331.1

The Langmuir model [28] assumes that adsorption takes place at specific homogeneous sites within the adsorbent; the saturated monolayer isotherm can be represented as:

$$q_e = \frac{q_m K_L C_e}{1 + K_L C_e} \tag{5}$$

where C_e (mg L^{-1}) is the equilibrium concentration, q_e (mg g^{-1}) is the amount of MB adsorbed onto per unit mass of CAMS at equilibrium; q_m (mg g^{-1}) is the maximum adsorption capacity related to monolayer coverage; and K_L (L mg^{-1}) is the Langmuir constant related to the affinity of the binding sites and energy of adsorption: the higher the K_L value, the higher the affinity of the binding sites.

From Table 1, it can be seen that the maximum adsorption capacity of CAMS (q_m) increases with the increasing of the temperature, while the values of K_L decrease with temperature rising. The values of q_m are 111.46, 114.4 and 156.6 mg g^{-1} at 293, 303 and 313 K, respectively.

According to Langmuir [29], the dimensionless constant separation factor R_L, which is the essential characteristic of the Langmuir isotherm, can be defined by:

$$R_L = \frac{1}{1 + K_L C_0} \tag{6}$$

The value of R_L for adsorption of MB onto CAMS was less than 1, whicht indicated that the adsorption behavior of CAMS was favorable for the MB.

The Freundlich model [30] can be expressed as:

$$q_e = K_F C_e^{1/n} \tag{7}$$

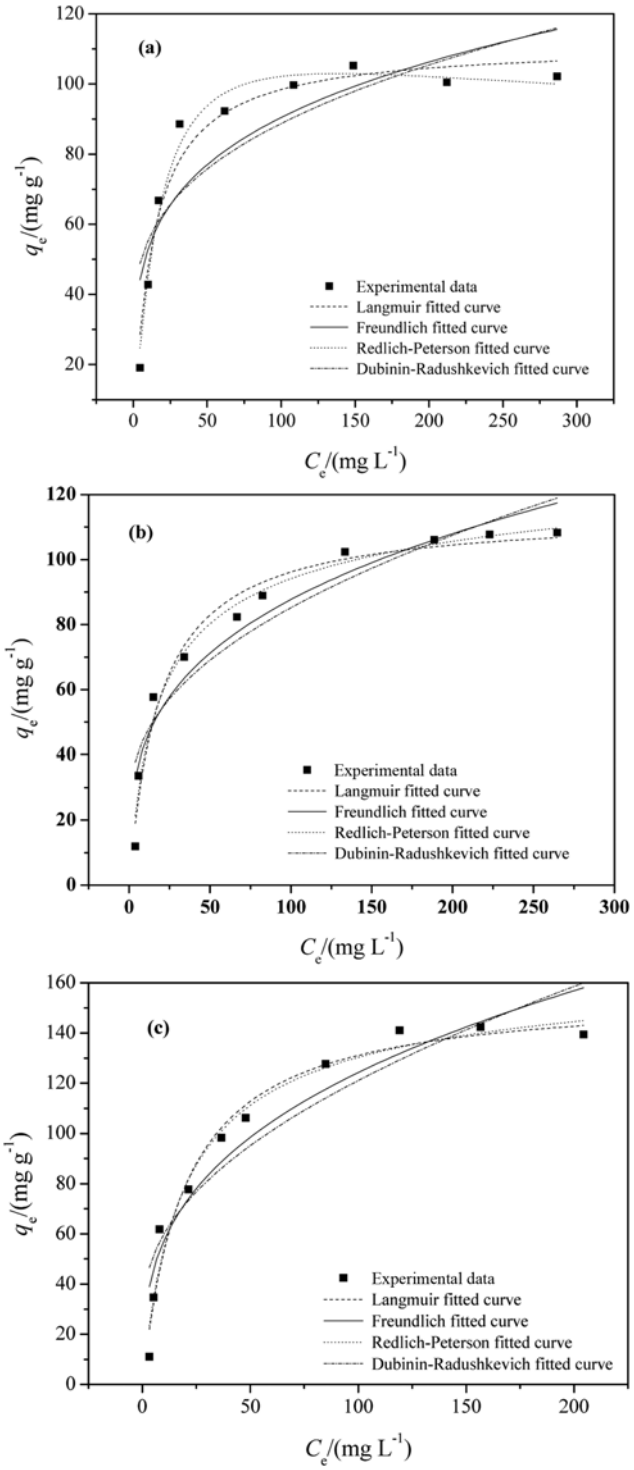

Fig. 10. The non-linear fitted curves with different equilibrium models at (a) 293 K, (b) 303 K and (c) 313 K, respectively.

where K_F is the Freundlich constant related to the adsorption capacity and 1/n is a indicator of adsorption intensity. The Freundlich equation is used to describe heterogeneous systems and reversible adsorption and is not restricted to the formation of monolayers [31]. Higher value for K_F indicates higher affinity for adsorbate and the values of the empirical parameter 1/n ($0.1<1/n<1$), indicates favorable adsorption [31]. Freundlich constants are given in Table 1. From

Table 1, the value of K_F decreased and 1/n increased with the increasing of temperature.

The Redlich-Peterson [32] model is given by Eq. (8):

$$q_e = \frac{AC_e}{1+BC_e^g} \quad (8)$$

where A, B and g are the Redlich-Peterson parameters, g lies between 0 and 1. Redlich-Peterson model is a compromise between Langmuir and Freundlich models. For g=1, Eq. (8) converts to the Langmuir form. Relevant adsorption parameters were also calculated according to the three-parameter isotherm of Redlich-Peterson at different temperatures, respectively. In this study, the constant g is near to 1, which means that the isotherms conformed to Langmuir model better than Freundlich model.

The Dubinin-Radushkevich [33] model is expressed as follows:

$$q_e = q_m \exp\left[\frac{(RT\ln(1+1/C_e))^2}{-2E^2}\right] \quad (9)$$

where q_m is the maximum adsorption capacity (mg g^{-1}) and E is energy of adsorption (kJ mol^{-1}), R is the gas constant (8.314×10^{-3} kJ mol^{-1} K^{-1}) and T is the absolute temperature (K). From Table 1, the energy of adsorption E (kJ mol^{-1}) decreased with the temperature increasing; the value of adsorption energy (E) indicated the nature of adsorption onto adsorbent. On the other hand, if the value of E was smaller than 8 kJ mol^{-1}, the nature of adsorption onto adsorbent was physical adsorption, whereas if the value of E was bigger than 8-16 kJ mol^{-1}, it was chemical adsorption [34]. In this study, the magnitude of E was higher than that 8 kJ mol^{-1} for all studied temperatures, indicating that the adsorption mechanism was chemical ion-exchange.

Based on the values of R^2, χ^2 and the experimental results in Table 1, the Langmuir isotherm appears to be the best model for the adsorption of MB onto CAMS at the different temperatures studied. The comparison of experimental points and fitted curves in Fig. 10 reinforces this result.

The calculated value of R_L in Table 1 indicate that the adsorption of MB on CAMS is favorable. Therefore, it indicates that a monolayer of MB covers the surface of adsorbent after adsorption.

Part of the data on MB sorption capacity (values of q_m derived from the Langmuir equation) of various adsorbents, especially the low cost adsorbents, is summarized in Table 2. Although the values of adsorption capacities were obtained at different experiment conditions, the results show that CAMS can be considered as a promising adsorbent for the removal of MB from aqueous solutions.

2-6. The Effect of Contact Time on Adsorption

The effect of contact time on the extent of MB adsorption onto CAMS shown in Fig. 11 indicates that a two-stage kinetic behavior was observed, with a very rapid initial adsorption over the first 200 min being followed by a longer period during which the uptake was considerably slower. At the start of the adsorption process, the values of q_t increased rapidly but then slowed down after 200 min. After 480 min, the quantity of MB adsorbed remained virtually constant. The phenomenon was probably due to the abundant availability of active sites on the surface of CAMS. Because of the gradual occupancy of these active sites, the dye sorption became less efficient.

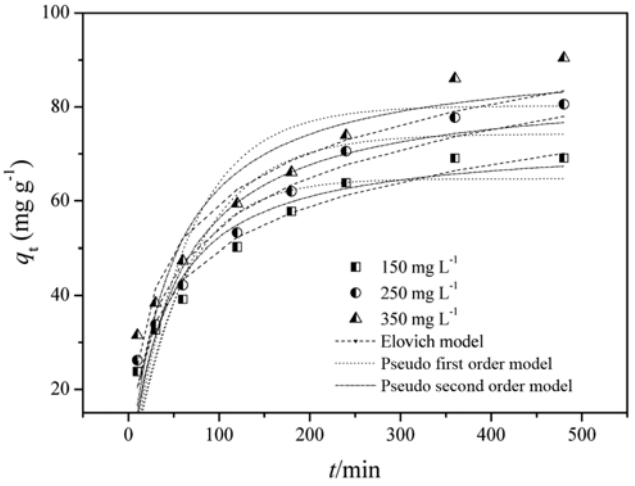

Fig. 11. Effect of contact time on adsorption of MB onto CAMS at 293 K.

It is also seen from Fig. 11 that higher initial dye concentration was an advantage of the increase in adsorption quantity. The q_t at equilibrium of MB adsorbed increased from 69 to 90 mg g^{-1} for an increase in dye concentration from 150 to 350 mg L^{-1}, respectively. This was probably due to the initial dye concentration providing a greater driving force, which led to greater concentration gradient, to overcome all mass transfer resistances of MB between the aqueous and solid phases.

2-7. Adsorption Kinetics

The kinetic models for the adsorption of MB onto CAMS were investigated by the application of the pseudo-first-order kinetic model, pseudo-second-order kinetic model and Elovich equation, respectively. The relative parameters of three kinetic models and values of R^2, χ^2 for adsorption of MB onto CAMS are listed in Table 3 using nonlinear regressive method, respectively. The fitted curves are also depicted in Fig. 11.

The pseudo-first-order equation may be expressed as the following equation [46]:

Table 2. The adsorption capacity q_m (mg g^{-1}) of MB of various adsorbents from the literature

q_m (mg g^{-1})	Adsorbent	References	q_m (mg g^{-1})	Adsorbent	References
111.46	CAMS	This paper	38.22	Hazelnut shell	[40]
99.0	Coconut husk	[35]	20.3	Cereal chaff	[41]
68.03	Peanut hull	[36]	18.6	Orange peel	[42]
42.3	Olive pomace	[37]	16.63	Wheat bran	[43]
40.6	Rice husk	[38]	16.05	Neem leaf	[44]
39.68	Cherry sawdust	[39]	8.76	Beech sawdust	[45]

Table 3. Kinetic parameters of MB adsorption onto CAMS

Parameter	C_o/(mg L^{-1})		
	150	250	350
Pseudo-first-order equation			
$k_1 \times 10^2$ (min^{-1})	1.817	1.457	1.591
q_e (exp) (mg g^{-1})	74.15	82.56	87.44
q_e (cal) (mg g^{-1})	64.74	74.26	80.23
R^2	0.8444	0.8316	0.7568
χ^2	54.12	81.47	131.8
Pseudo-second-order equation			
$k_2 \times 10^3$ (g mg^{-1} min^{-1})	0.350	0.230	0.240
q_e (cal) (mg g^{-1})	72.93	84.76	90.97
h (mg g^{-1} min^{-1})	1.699	1.653	2.054
R^2	0.9291	0.9124	0.8685
χ^2	24.66	42.36	71.24
Elovich equation			
A	−9.447	−13.945	−9.906
B	12.89	14.89	15.12
R^2	0.9873	0.9814	0.9751
χ^2	2.9565	4.1645	4.9093
Intraparticle diffusion model			
k_{i1} (mg g^{-1} $min^{-0.5}$)	3.292	3.577	3.373
C_1 (mg g^{-1})	13.88	14.48	20.89
R	0.9996	0.9996	0.9983
k_{i2} (mg g^{-1} $min^{-0.5}$)	0.776	1.252	1.401
C_2 (mg g^{-1})	53.31	51.45	51.58
R	0.9404	0.9927	0.9158

$$q_t = q_e(1 - e^{-k_1 t}) \tag{10}$$

where q_e and q_t (mg g^{-1}) are the MB adsorption capacity at equilibrium and at time t (min), respectively, and k_1 (min^{-1}) is the rate constant of the pseudo-first-order.

The pseudo-second-order kinetic model is given by the following equation [47]:

$$q_t = \frac{k_2 q_e^2 t}{1 + k_2 q_e t} \tag{11}$$

where k_2 (g mg^{-1} min^{-1}) is the rate constant of pseudo-second-order adsorption.

The Elovich equation is expressed as the following equation [48]:

$$q_t = A + B \ln t \tag{12}$$

where A and B are the Elovich constant.

Based on the values of R^2 and χ^2 listed in Table 3 and the experimental data depicted in Fig. 11, the Elovich equation had a high degree of fitting. As the Elovich equation is successfully used to describe the adsorption kinetics of ion exchange systems, it can be concluded that the adsorption system is a chemical process, especially an ion exchange process [48]. There was negative charge of carboxyl group ($-COO^-$) on the surface of CAMS, but MB existing in solution were positive. So it was inferred that the main mechanism of MB adsorption behavior by CSMS may be ion exchange. This result is also consistent with the foregoing conclusion derived from the mean free energy of adsorption (E) in the D-R isotherm.

3. Adsorption Mechanism

The adsorbate transport from the solution phase to the surface of the adsorbent particles occurs in several steps. The overall adsorption process may be controlled by one or more steps. The possibility of intra-particle diffusion was explored by using the intra-particle diffusion model [48]:

$$q_t = k_i t^{0.5} + C \tag{13}$$

where q_t (mg g^{-1}) is the amount of MB adsorbed at time t, k_i (g mg^{-1} $min^{-0.5}$) is the intra-particle diffusion rate constant and C is a constant regarding the thickness of the boundary layer, which is in direct ratio to the effect of the boundary layer.

The values of k_i and C were obtained from the slope and intercept of the linear plot of q_t versus $t^{0.5}$. If the line passes through the origin, the intra-particle diffusion will be the sole rate limiting step. If the line does not pass through the origin, it implies that intra-particle diffusion is not the sole rate control step, and other processes may control the rate of adsorption [7].

The plot of q_t versus $t^{0.5}$ for MB adsorption on CAMS is shown in Fig. 12; the values of k_i and C are in Table 3.

It can be seen from Fig. 12 that the experimental data points show two linear sections with different slopes, which indicates the different stages in adsorption. For all two-linear plots in Fig. 12, the regression estimates of the first linear segments have intercept values different from zero, which consistent with the value of C shown in Table 3, suggesting pore diffusion not be the step controlling the overall rate of mass transfer at the beginning of batch adsorption. So the adsorption process may be of a complex nature consisting of both surface adsorption and intra-particle diffusion [49]. Film-diffusion control may also have occurred during these early stages of the adsorption process and may have still been controlling the rate of mass transfer during the time period of the first linear segment [50]. This shows that both the surface adsorption and intra-particle diffusion contributed to the actual adsorption process. As given in Table 3, it is obvious that values of the pore diffusion rate parameters increased with the initial dye concentration increasing. The in-

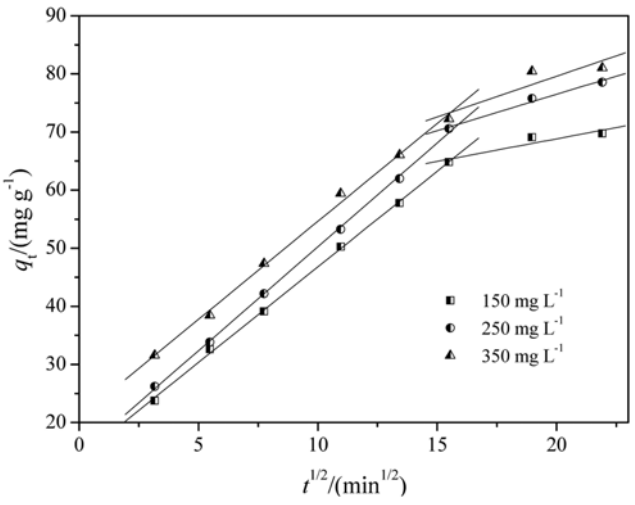

Fig. 12. Intra-particle diffusion plots for MB adsorption of onto CAMS.

creasing in dye concentration resulted in the driving force increasing, which increased the diffusion rate of the molecular dye in the pores [51]. It was also observed that the values of C increased with the initial concentration of the dyes, indicating an increasing in the thickness and the effect of the boundary layer.

To confirm the actual rate-limiting steps involved in the MB adsorption process, the kinetic data were further analyzed; the initial (D_i) and the final (D_f) diffusion coefficients, which assumed a particle diffusion mechanism to be rate-limiting, were calculated using the expression as following given by [52]:

$$F = 1 - \frac{6}{\pi^2}\sum_{n=1}^{\infty}\frac{1}{n^2}\exp\left(-\frac{D \cdot n^2 \pi^2 \cdot t}{r_0^2}\right) \quad (14)$$

where F is the fractional attainment of equilibrium at time t of the amount of the exchanged cations given by:

$$F = \frac{q_t}{q_\infty} \quad (15)$$

D is the diffusion coefficient, r_0 is the radius of the adsorbent particle assuming a spherical shape and n is an integer (20-40 mesh, 30 mesh was chosen).

In the case of short operating times, Eq. (14) can be rearranged to:

$$\frac{q_t}{q_\infty} = \frac{6}{r_0}\left(\frac{D_i t}{\pi}\right)^{0.5} \quad (16)$$

The initial diffusion coefficients D_i were obtained from plots of q_t/q vs. $t^{0.5}$. In this paper, q_e values at 480 min of exchanged CAMS were rearranged as q_∞ values. The gradient (p_1) of the initial linear portion of this curve was used typically up to (q_t/q=0.4-0.6) and it was given by the following expression:

$$p_1 = \frac{6}{r_0}\left(\frac{D_i}{\pi}\right)^{0.5} \quad (17)$$

It means that the coefficient D_i becomes:

$$D_i = \frac{p_1^2 \pi r_0^2}{36} \quad (18)$$

The values of the D_i are listed in Table 4. As given there, it is obvious that value of D_i increased with the increasing initial MB concentration.

In the case of longer operating times, Eq. (14) can be rearranged:

$$\ln\left(1 - \frac{q_t}{q_\infty}\right) = \ln\left(\frac{6}{\pi^2}\right) - \left(\frac{D_f}{r_0^2}\right) \cdot \pi^2 \cdot t \quad (19)$$

Table 4. Coefficients diffusion D_i and D_f values of exchanged CAMS at different initial MB concentrations

Parameter	C_o/(mg L^{-1})		
	150 mg L^{-1}	250 mg L^{-1}	350 mg L^{-1}
$D_i \times 10^8$ (cm^2 s^{-1})	4.467	6.21	6.59
R	0.9751	0.9893	0.9975
SD	0.0376	0.0289	0.0142
$D_f \times 10^7$ (cm^2 s^{-1})	1.553	2.134	2.668
R	0.9378	0.9750	0.9948
SD	0.1087	0.0921	0.0518

where D_f is the final diffusion coefficient. The values of D_f can be calculated by the determination of the gradient (p_2) from plots ln [$(1-q_t/q_e)$] vs. t (min).

$$p_2 = \frac{D_f}{r_0^2} \cdot \pi^2 \quad (20)$$

The coefficient D_f become:

$$D_f = \frac{p_2 \cdot r_0^2}{\pi^2} \quad (21)$$

The values of D_f are also listed in Table 4, which were calculated at different dye concentrations. This result may explain the difference between film diffusion and particle diffusion limiting adsorption process [45]. Table 4 shows that D_f increased with the increasing initial MB concentrations. It also shows that the diffusion coefficients D_i were smaller than D_f, suggesting that initial rate of exchange was almost always smaller than final rate of exchange [45].

According to Singh et al. [53], if the order of D value is 10^{-10}-10^{-11} cm^2 s^{-1}, intra-particle diffusion is the rate-limiting step in the adsorption process. In this paper, the order of D_i and D_f value obtained was 10^{-7} cm^2 s^{-1}, which is three orders of magnitude greater than the value quoted by Singh et al. This indicates that intra-particle diffusion was not the sole rate-limiting step.

4. Calculation of Thermodynamic Parameters

Thermodynamic parameters are important in adsorption studies to determine whether a given process will occur spontaneously.

The Gibbs free energy change (ΔG), enthalpy change (ΔH) and entropy change (ΔS) were calculated by the following equations:

$$\Delta G = -RT \ln K_c' \quad (22)$$

The value of ΔH and ΔS can be obtained from the slope and intercept of a van't Hoff equation of ΔG versus T.

$$\Delta G = \Delta H - T\Delta S \quad (23)$$

where R (8.314 J $mol^{-1}K^{-1}$) is gas constant and T (K) is absolute temperature.

The apparent equilibrium constant (K_c') of the adsorption is defined as:

$$K_c' = C_{ad,e}/C_e \quad (24)$$

where $C_{ad,e}$ is the concentration of adsorbate on the adsorbent at equilibrium (mg L^{-1}). The K_c' value is used in Eq. (22) to obtain the value of ΔG [10,14].

The values of ΔG for MB were −12.68, −12.95 and −13.67 kJ mol^{-1} at 293,303 and 313 K, respectively. The value of ΔH and ΔS was 1.899 kJ mol^{-1} and 0.495 kJ mol^{-1} K^{-1}, respectively. The values of ΔG were negative at the various temperatures, indicating that the adsorption process was spontaneous. Besides, the negative value of ΔG decreased with the increasing temperature, indicating that adsorption of MB onto CAMS became more favorable at higher temperature. The increase in the adsorption capacity of the adsorbent at higher temperatures may be due to an enlargement of the pore size or activation of the adsorbent surface. The positive value of H indicated that the adsorption process was endothermic. The positive value of ΔS confirmed the increasing randomness at the solid-solute interface during adsorption of MB on the active sites of CAMS

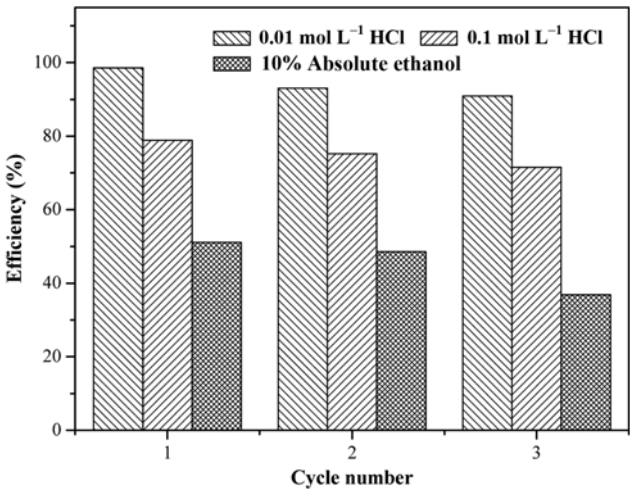

Fig. 13. The regeneration of CAMS (C_0=250 mg L^{-1}; CAMS dosage=2 g L^{-1}; 480 min; 293 K; pH=6.5).

and also reflected the affinity of the adsorbent for the dye.

5. Regeneration

Regeneration of spent adsorbent and recovery of adsorbate would make the treatment process economical. It may decrease the process cost and also the dependency of the process on a continuous adsorbent supply. For this purpose, it is desirable to desorb the adsorbed dyes and to regenerate the adsorbent for another cycle of application. The selected eluent must be effective, innoxious for the biosorbent, non-polluting, and low-cost. In this study, MB-loaded adsorbents were exposed to three different eluants: HCl and absolute ethanol. The results are illustrated in Fig. 13. As seen in Fig. 13, at the first cycle, the eluants of 0.01 mol L^{-1} HCl performed well with MB-removal efficiencies around 98%. However, the eluants of 0.1 mol L^{-1} HCl and 10% absolute ethanol exhibited poor performance, with MB-removal efficiencies around 78% and 51%, respectively. The second and third cycle showed a decreased efficiency for all the eluants, while the MB-removal efficiency being exposed to 0.01 mol L^{-1} HCl was still over 90%. Therefore, desorption and subsequent reuse was possible with MB-loaded adsorbents being exposed to the eluant of 0.01 mol L^{-1} HCl, since it exhibited both good MB uptake capacity and easy desorption in all three subsequent cycles examined.

CONCLUSIONS

The ability of sawdust modified with citric acid to remove MB was investigated. The results indicated that the adsorption capacity of the adsorbent was strongly affected by the initial pH of solutions, the initial dye concentration, the amount of adsorbent and temperature. The adsorption capacity of CAMS increased with the initial dye concentration, temperature and the initial pH, but it decreased with the increasing of adsorbent dosage and the salt concentration. The isothermal data followed the Langmuir model best. The Elovich rate equation best fitted the adsorption process. The mechanism of the adsorption process was found to be complex, consisting of both surface adsorption and pore diffusion. The thermodynamic study indicated that the adsorption of dyes was spontaneous and endothermic. After desorption with 0.01 mol L^{-1} HCl, CAMS could be reused to adsorb MB at least three cycles. Based on these results, we concluded that CAMS could be used as a low-cost, effective and reproducible adsorbent for the removal of MB dye from aqueous solution.

ACKNOWLEDGEMENTS

This work was supported by the Education Department of Henan Province in China (No. 2010A610003) and Henan Science and Technology Department in China (No. 102102210103).

REFERENCES

1. D. Fatih and K. Sengul, *Chem. Eng. J.*, **170**, 67 (2011).
2. V. K. Gupta and Suhas, *J. Environ. Manage*., **90**, 2313 (2009).
3. Y. M. Slokar and A. Majcen Le Marechal, *Dyes Pigm.*, **37**, 335 (1998).
4. A. E. Ofomaja. *Chem. Eng. J*., **143**, 85 (2008).
5. R.Sivaraj, C. Namasivayam and K. Kadirvelu, *Waste Manage*., **21**, 105 (2001).
6. N. Nasuha and B. H. Hameed, *Chem. Eng. J.*, **166**, 783 (2011).
7. R. M. Gong, S. X. Zhu, D. M. Zhang, J. Chen and S. J. Ni, *Desalination*, **230**, 220 (2008).
8. D. Özer, G. Dursun and A. Özer, *J. Hazard. Mater*., **144**, 171 (2007).
9. S. Gupta, D. Kumar and J. P. Gaur, *Chem. Eng. J*., **148**, 226 (2009).
10. W. H. Zou, H. J. Bai, K. Li and X. L. Shi, *Adsorp. Sci. Technol.*, **28**, 641 (2010).
11. K. K. Wong, C. K. Lee, K. S. Low and M. J. Haron, *Chemosphere*, **50**, 23 (2003).
12. M. Šćiban, B. Radetiæ, Ž. Kevrešan and M. Klašnja, *Bioresour. Technol.*, **98**, 402 (2007).
13. H. Zhang, Y. Tang, X. N. Liu, Z. G. Ke, X. Su, D. Q. Cai, X. Q. Wang, Y. D. Liu, Q. Huang and Z. L. Yu, *Desalination*, **274**, 97 (2011).
14. T. Vaughan, C. W. Seo and W. E. Marshall, *Bioresour. Technol.*, **78**, 133 (2001).
15. P. C. C. Faria, J. J. M. Órfão and M. F. R. Pereira, *Water Res.*, **38**, 2043 (2004).
16. I. Irbe, B. Anderson, J. Chirkova, U. Kallavus, I. Anderson and O. Faix, *Int. Biodeterior. Biodegrad*, **57**, 99 (2005).
17. R. P. Han, L. J. Zhang, C. Song, M. M. Zhang, H. M. Zhu and L. J. Zhang, *Carbohyd. Polym.*, **79**, 1140 (2010).
18. C. R. T. Tarley and M. A. Z. Arruda, *Chemosphere*, **54**, 987 (2004).
19. K. K. Krishnani, X. G. Meng, C. Christodoulatos and V. M. Boddu, *J. Hazard. Mater*., **153**, 1222 (2008).
20. Z. Wang, J. Cao and J. Wang, *J. Anal. Appl. Pyrol*., **84**, 179 (2009).
21. V. K. Garg, R. Kumar and R. Gupta, *Dyes Pigm.*, **63**, 243 (2004).
22. S. Senthilkumaar, P. R. Varadarajan, K. Porkodi and C. V. Subbhuraam, *J. Colloid Interface Sci*., **284**, 78 (2005).
23. S. Özcan, B. Erdem and A. Özcan, *Colloid Surf. A.*, **266**, 73 (2005).
24. N. Nasuha, B. H. Hameed and A. T. Mohd Din, *J. Hazard. Mater*., **175**, 126 (2010).
25. G. Moussavi and R. Khosravi, *Chem. Eng. Res. Des*., **89**, 2182 (2011).
26. C. A. P. Almeida, N. A. Debacher, A. J. Downs, L. C. Cottet and A. D. Mello, *J. Colloid Interface Sci*., **332**, 46 (2009).
27. J. Sánchez-Martín, M. González-Velasco, J. Beltrán-Heredia, J.

Gragera-Carvajal and J. Salguero-Fernández, *J. Hazard. Mater*., **174**, 9 (2010).
28. L. Langmuir, *J. Am. Chem. Soc*., **38**, 2221 (1916).
29. L. Langmuir, *J. Am. Chem. Soc*., **40**, 1361 (1918).
30. H. M. F. Freundlich, *J. Phys. Chem*., **57**, 385 (1906).
31. A. S. Özcan, B. Erdem and A. Özcan, *J. Colloid Interface Sci*., **280**, 44 (2004).
32. O. Redlich and D. L. Peterson, *J. Phys. Chem*., **63**, 1024 (1959).
33. M. M. Dubinin, *Chem. Rev*., **60**, 235 (1960).
34. D. Nibou, S. Khemaissia, S. Amokrane, M. Barkat, S. Chegrouche and A. Mellah, *Chem. Eng. J*., **172**, 296 (2011).
35. K. S. Low and C. K. Lee, *Pertanika*, **13**, 221 (1990).
36. R. M. Gong, Y. Z. Sun, J. Chen, H. J. Liu and C. Yang, *Dyes Pigm.*, **67**, 175 (2005).
37. M. Rafatullah, O. Sulaiman, R. Hashim and A. Ahmad, *J. Hazard. Mater*., **177**, 70 (2010).
38. V. Vadivelan and K. V. Kumar, *J. Colloid Interface Sci*., **286**, 90 (2005).
39. H. Lata, V. K. Garg and R. K. Gupta, *Dyes Pigm*., **74**, 653 (2007).
40. M. Dogan, H. Abak and M. Alkan, *Water, Air, Soil Pollut*., **192**, 141 (2008).
41. R. P. Han, Y. F. Wang, P. Han, J. Shi, J. Yang and Y. S. Lu, *J. Hazard. Mater*., **137**, 550 (2006).
42. G. Annadurai, R. S. Juang and D. J. Lee, *J. Hazard. Mater*., **92**, 263 (2002).
43. X. S. Wang, Y. Zhou, Y. Jiang and C. Sun, *J. Hazard. Mater*., **157**, 374 (2008).
44. K. G. Bhattacharyya and A. Sharma, *Dyes Pigm.*, **65**, 51 (2005).
45. F. A. Batzias and D. K. Sidiras, *J. Hazard. Mater*., **114**, 167 (2004).
46. Y. S. Ho, J. C. Y. Ng and G. McKay, *Sep. Purif. Methods*, **29**, 189 (2000).
47. Y. S. Ho and G. McKay, *Chem. Eng. J*., **70**, 115 (1998).
48. C. W. Cheung, J. F. Porter and G. McKay, *Sep. Purifi. Technol*., **19**, 55 (2000).
49. V. Vadivelan and K. V. Kumar, *J. Colloid Interface Sci*., **286**, 90 (2005).
50. V. C. Srivastava, M. M. Swamy, I. D. Mall, B. Prasad and I. M. Mishra, *Colloids Surf*., **272**, 89 (2006).
51. W. H. Zou, K. Li, H. J. Bai, X. L. Shi and R. P. Han, *J. Chem. Eng. Data*., **56**, 1882 (2011).
52. G. E. Boyd, A. W. Adamson and L. S. Myers, Jr. *J. Am. Chem. Soc*., **69**, 2836 (1947).
53. K. K. Singh, R. Rastogi and S. H. Hasan, *J. Colloid Interface Sci*., **290**, 61 (2005).